J Mater Sci (2011) 46:4545–4554
DOI 10.1007/s10853-011-5349-3

Characterization of damping in carbon-nanotube filled fiberglass reinforced thermosetting-matrix composites

R. J. Johnson · J. Tang · R. Pitchumani

Received: 11 November 2010 / Accepted: 29 January 2011 / Published online: 11 February 2011

Abstract Use of carbon nanotubes as additives to composite parts for the purpose of increased damping has been the subject of much recent attention, owing to their large surface area per weight ratio which provides for frictional losses at the carbon nanotube–resin matrix interface. This article presents an experimental study to quantify the structural damping in composites due to the addition of carbon nanotubes to thermosetting resin systems with and without fiberglass reinforcement. Carbon nanotubes of varying quantity and morphology are ultrasonically dispersed in epoxy resin and are compression molded to form test samples that are used in forced vibration, free vibration with initial tip deflection, and tension tests to determine their damping ratio, specific damping capacity, and Young's modulus. Results show increased stiffness and specific damping capacity with the addition of carbon nanotubes and particularly increased frictional loss with increasing surface area to weight ratio. The addition of fiberglass reinforcement to composite samples is shown to reduce the effective damping ratio over plain epoxy samples and carbon nanotube-filled epoxy samples.

This study was funded by the National Science Foundation through Grant nos. CBET-0522933 and CBET-0934008.

R. J. Johnson
ASML, Wilton, CT, USA

J. Tang
Department of Mechanical Engineering,
University of Connecticut, Storrs, CT, USA

R. Pitchumani (✉)
Department of Mechanical Engineering, Advanced Materials and Technologies Laboratory, Virginia Tech,
Blacksburg, VA 24061-0238, USA
e-mail: pitchu@vt.edu
URL: http://www.me.vt.edu/amtl

Introduction

Composites made of thermosetting epoxy resin with fiberglass reinforcement offer a lightweight, strong, fatigue resistant alternative to metals for many applications. Such composites have been well received in the marine industry for years and more recently in the automotive industry for select body panels. Similar composites with advanced reinforcing fibers made of carbon or Kevlar are more widely used in the aerospace and sporting goods industries. Many of these applications could benefit from structural components with increased vibration damping characteristics, so as to alleviate noise and other unwanted vibrations and, in turn, improve dynamic performance. Viscoelastic polymer coatings [1, 2] are often used to achieve large damping; however, these systems suffer from some drawbacks including large weight, reduced performance at high temperature, and geometric size penalties. Recently, much research has been performed on carbon nanotube additives to polymers, forming composite structures with improved physical properties including strength, thermal conductivity, and damping [3–7].

Owing to their impressive strength and high elastic modulus carbon nanotubes are attractive nanoscale reinforcements for polymeric composites and much research has attempted to harness this strength with some success [3, 8, 9]. A limitation, however, lies in the interface between the carbon nanotube and the polymer matrix material; while a good interface leads to increased strength, weak interfaces have been hypothesized in the literature to lead to an interfacial slipping motion and associated friction,

which can be utilized to improve damping in composite structures or create polymer coatings that do not suffer from the thermal or weight problems of other viscoelastic materials. Carbon nanotube-based damping improvements can also be attributed to nanotube–nanotube interactions at high concentrations, the breaking of functional bonds between polymers and carbon nanotubes [10], and the modification of the polymer chemical structure itself becaus of the carbon nanotubes [11–13].

Recent investigations on this topic have been performed by various research groups [6, 10, 14–19]. Zhou et al. [6] reported that at low weight %, carbon nanotube fillers increase damping through a stick-slip type friction at the surface of the nanotubes, and consequently, the interfacial surface area is a major factor. Koratkar et al. [14] measured the damping enhancement of single-walled carbon nanotubes in polycarbonate samples using uniaxial tension testing, shear testing of multiwalled carbon nanotube thin films [19] and also reported on the effects of temperature on the critical stress above which the major advantages of carbon nanotube stick-slip friction are evident [15]. Investigations of closely packed chemical vapor deposited multi-walled carbon nanotubes were performed where the thin film displayed enhanced damping because of nanotube–nanotube interactions [16]. Single-walled carbon nanotubes added to an epoxy base were investigated using uniaxial tension testing [10] and vibration of cantilever beams [6], and the data was used to validate a stick-slip friction model of carbon nanotube dissipation in polymers. Carbon nanotube loaded epoxy has also been used as an adhesive between two metal plates forming a laminate beam. Free and forced vibration experiments performed on these beams show a close match in the vibrational envelope to a closed form solution to the nonlinear equations of motion [17, 18].

The goal—and principal contribution—of this article is that of characterizing the damping behavior of glass fiber reinforced composites with added carbon nanotubes, with potential use as integral passive damping elements in structural composite applications including rotocraft structures. As evident from the aforementioned literature references, little has been reported on the damping characteristics of conventional composites incorporating carbon nanotubes. Carbon nanotubes offer excellent surface area to weight ratios typically in the range of 714–1709 m^2/g when compared to carbon black or carbon whiskers with surface area to weight ratios on the order of $\sim$10–0.4 m^2/g, respectively [20]. A systematic study is conducted on the effects of carbon nanotube morphology (single-walled nanotubes and multi-walled nanotubes), nanotube loading and aspect ratio, all of which govern the interfacial surface area, on the damping behavior of a glass fiber-reinforced thermosetting matrix composite. The article is organized as follows: Experimental studies outlines the experimental procedures including sample preparation as well as the testing of the samples. Data analysis and results of the experimental studies are presented in Results and discussion followed by Conclusions.

Experimental studies

The goal of the experimental studies is to determine the increase in damping that occurs as a result of adding carbon nanotubes to a thermosetting resin with and without fibrous reinforcements. The studies focus on measuring the changes in damping and elastic properties because of the addition of single-walled (SWCN) and multi-walled carbon nanotubes (MWCN) of various geometries, as listed in Table 1, to a composite comprised of Owens Corning M8610 continuous random fiber mat at a fiber volume fraction of 0.18 and EPON 828 epoxy resin catalyzed with EPICURE 3274 curing agent (from Hexion Specialty Chemicals, Columbus, OH, USA). Single-walled carbon nanotubes which were obtained from SES Research, Inc. (Houston, TX, USA) having a purity of 20–40%, and three geometries of multi-walled, research grade (>95% purity) carbon nanotubes were obtained from NanoLab, Inc. (Newton, MA, USA) having nominal aspect ratios ranging from 100 to 833. The aspect ratio of the carbon nanotubes was determined from calculations based on the length and diameter reported by the manufacturer and does not include any breakage that may result from sample preparation. However, it is generally expected that since all the samples are subjected to the same processing conditions, even with breakage, the relative ordering of the aspect ratio among the various samples will be preserved.

In all of the studies, 0, 1, and 2 wt% carbon nanotube loadings were considered. In addition, samples without fiber reinforcement were produced with and without the addition of 2 wt% single-walled carbon nanotubes to determine the effects of the fiber on the increased damping brought about by carbon nanotube fillers. Sine sweep and free vibration tests with initial tip deflection on cantilever beams were used to measure the damping ratio and the ASTM 638 plastic tension test [21] was used to measure the modulus. The sample preparation and the tests conducted are described in the following subsections.

Sample preparation

To insure uniformity of carbon nanotube dispersion in the reinforced composite samples as well as neat resin specimens, all samples were fabricated using compression molding techniques, in which the resin flows through the thickness of the part as it is being compressed. Both ASTM

Table 1 Carbon nanotube geometries considered in the study

Type	Diameter (nm)	Length (μm)	Nominal aspect ratio	Surface area to weight ratio (m^2/g)
MWCN	30 ± 15	1–5	100	74
MWCN	30 ± 15	5–20	416	74
MWCN	15 ± 5	5–20	833	148
SWCN	~1.3	~10	7692	1709

638 specimens and cantilever beam samples were formed by the compression molding process.

First, appropriate amounts of carbon nanotubes and EPON 828 resin were weighed using an Ohaus Explorer Pro precision balance (Ohaus Corporation, Pine Brook, NJ, USA) and hand mixed. The mass of carbon nanotubes was selected to yield 0, 1 or 2 wt% of nanotubes in the mixture of resin and curing agent. Next the carbon nanotubes were dispersed in the resin using a Cole-Parmer 500 watt ultrasonic processor (Cole-Parmer Instrument Company, Vernon Hills, IL, USA) with a 1/4 in microtip. The sample container was placed in a water bath during sonification to avoid heat build up, and the sample was sonified at 20% amplitude in a pulsed on-off mode with 1 s pulses for a total duration of 1 h. The technique insured that the sample temperature never exceeded 50 °C during sonification. The carbon nanotube loaded resin system was degassed in a vacuum at 25 in Hg for 15 min to remove entrapped air from sonification prior to compression molding. The carbon nanotube-filled EPON 828 resin was hand mixed with EPICURE 3274 to form a 100:40 by weight ratio of resin to curing agent as recommended by the manufacturer.

Compression molding was carried out using a three part aluminum mold consisting of a separable top section, a middle spacer frame, and a bottom plate, as shown in Fig. 1a. The bottom section was sealed to the middle spacer using an O-ring held in place by a groove in the lower mold. The middle and bottom sections were bolted together, effectively flattening the O-ring into its grove, prior to the addition of fiber and resin-curing agent-nanotube mixture. The cavity formed by the mold measured $3.7 \times 38.1 \times 165.1$ mm^3. The top section was sealed to the middle spacer frame-bottom section assembly using another O-ring held in a channel on the top side of the spacer frame. The mold top had an inverted hat shape with a lip around the outer edge that landed on the middle spacer section and insured part thickness control. Holes in the lip allowed clearance for the bolts used to assemble the lower two sections. The central hat portion of the mold top engaged inside the cavity created by the middle spacer frame, to compact the reinforcing preform during the compression stage.

Prior to assembly, the mold components were sprayed with a Teflon (PTFE) mold release to aid in removal of the produced specimens. A precisely measured volume of the carbon nanotube-filled catalyzed resin system described above was added to the assembled middle and bottom sections of the mold followed by two layers of Owens Corning M8610 random fiber mat for the fiber reinforced samples. The top section of the mold was then aligned and engaged with the middle spacer and the assembled structure was placed in a Tetrahedron MTP-10 programmable hot press and compression molded at a uniform force of 5000 lbf. The mold was subject to a cure temperature cycle that ramped up from room temperature to 93 °C in 5 min, held constant for a period of 1 h, and ramped down to room temperature over a duration of of 15 min. Compression molded rectangular plates of carbon nanotube-filled resins with and without fiberglass reinforcements were removed from the mold and computer numerical control (CNC) machined to form a single $12.7 \times 152.4 \times 3.7$ mm^3 cantilever beam and two ASTM 638 type V specimens [21], as shown in Fig. 1b. Figure 1b shows the as-machined sample, and Fig. 1c and d shows the cantilever beam specimen and ASTM 638 specimen, respectively. In Fig. 1c and d, the lighter colored specimens are pictures of samples without carbon nanotubes while the darker colored samples in the foreground of the pictures are carbon nanotube-filled specimens. The specimens were fabricated for a wide range of carbon nanotube morphologies and dimensions as provided in the first three columns of Table 1. The Table also lists the nominal aspect ratio (obtained as the ratio of the mean of the length range to the mean of the diameter) and the surface area to weight ratio (computed using the nominal geometry of the carbon nanotubes and the density of carbon).

Composite plates fabricated by compression molding include: one plate with no carbon nanotube filler or fiberglass reinforcement, one plate with 2 wt% single-wall carbon nanotubes and no fiberglass reinforcement, and nine plates with fiberglass reinforcement including one with no carbon nanotube fillers, and eight that consist of one each of the four geometries of carbon nanotubes studied (listed in Table 1) at 1 and 2 wt% loadings. All compression molded composite plates with carbon nanotubes were sectioned and examined under a scanning electron microscope to verify uniformity of carbon nanotube dispersion. No agglomeration of the carbon nanotubes was seen

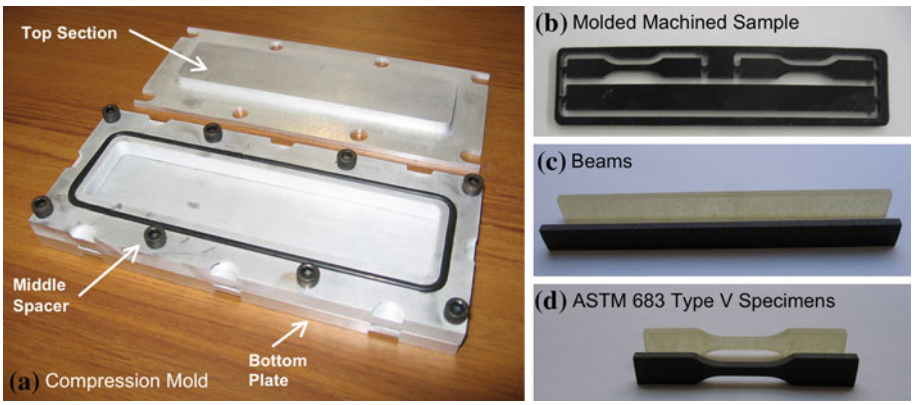

Fig. 1 **a** Compression mold with 6.5 × 1.5 × 0.125 inch cavity used to make the test specimens. **b** Photograph of a machined plate consisting of a cantilever beam specimen and two ASTM 638 type V specimens; **c**, **d** are photographs of the individual specimens cut from the frame and polished

indicating that the ultrasonic dispersion was effective for the range of carbon nanotube weight fractions considered. Each composite plate yielded two ASTM 638 type V specimens and one beam specimen, which were used in the experiments described in the following subsections.

Vibration experiments

Forced vibration tests and free vibration tests with initial tip deflection were performed on the cantilever beam samples to obtain frequency response and decay envelope data, respectively. Forced vibration tests, also referred to as the sine sweep tests, utilized a Ling 100 electrodynamic shaker, powered by a Crown CE2000 amplifier, with signal generated by an Agilent 35670A signal analyzer. The cantilever beam was held by an in-house fabricated steel clamp attached to the shaker armature, and the base and tip accelerations were measured using PCB 352C23 accelerometers (PCB Piezotronics, Inc.). Frequency was swept from 5–5000 Hz at a fixed peak-to-peak voltage and amplifier gain while the tip and base accelerations of the beam were measured to determine the frequency response.

Free vibration with initial tip deflection tests were carried out on the beam samples to measure the decay of the vibration envelope. The beams were clamped with an in-house fabricated fixture in a cantilever configuration where the beam length was selectable by changing the depth of insertion of the beam sample into the fixture. A PCB 352C23 accelerometer was mounted at the beam tip and connected to an Agilent 35670A signal analyzer programed to capture 1 s of acceleration data at 5kHz sampling rate, triggered by the accelerometer input. The beam was manually deflected and systematically released using a digital caliper mounted in a machine vice that functioned to initially hold the beam deflection and then as the vise was slid away, release the beam from a highly accurate displaced position with zero initial velocity. Individual tests were repeated 5 times and the data averaged to increase statistical precision. Free vibration with initial tip deflection tests were performed for beam lengths of 3.5–5 inches at every 0.5 inch interval for initial tip deflections of 5, 10, and 20 mm. The data reduction and analysis procedure for these experiments is discussed in Results and discussion.

Tensile testing

Tensile testing experiments were performed on the machined specimens shown in Fig. 1c following ASTM Standard 638 [21] for tensile testing of plastics and composite materials. The test specimens were of type V defined in the ASTM standard and were pulled at the specified rate of 0.05 in/min in an INSTRON 5869. Strain data was obtained over a 0.5 inch gauge length using an INSTRON 2630 series extensometer. Each experiment was performed 5 times over a 0–2% strain range. Data was captured at a rate of ten points per second and the first 20 points in each set were used as the initial part of the stress-strain data to obtain a least-squared linear fit, the slope of which was measured as the Young's modulus, E.

Results and discussion

The results of the experimental studies are presented in this section, organized as follows: the results of the forced vibration tests are first presented followed by the results of the free vibration with initial tip deflection tests, and the tensile test results. In each case, the effects of carbon nanotubes are systematically elucidated.

Forced vibration experiments were conducted in the form of a sine sweep using the cantilever beam specimens with 0, 1, and 2 wt% loadings of the carbon nanotube types listed in Table 1, fabricated both with and without fiber reinforcement. The resulting frequency response, which is a measure of the tip acceleration to the base acceleration, is plotted in Fig. 2 for three carbon nanotube loadings (0, 1, and 2 wt%) of 30 nm diameter 1–5 μm length multi-walled carbon nanotubes in samples produced with fiber

reinforcement, tested at 5 inch beam length. The response demonstrates three clear frequency peaks with a shift toward higher frequency for increased carbon nanotube loading. This positive shift of the natural frequencies indicates increased stiffness of the samples. The peak amplitude and width of the peaks, which directly correspond to the damping in the beams, is not significantly altered; this trend was seen for other geometries of carbon nanotubes studied here but are not shown. Therefore, determination of the damping ratio through the half-power method [22] or correlation of the experimental data to a finite element model [23] is less reliable from the forced vibration test data. It should be noted that the forced vibration experiments were done at a sampling frequency of 5 kHz, which limits the analysis to a 2.5 kHz frequency resolution. Since the analysis presented focuses only on the first few modes, the sampling frequency used is adequate and is not a limitation for the study reported. A higher sampling frequency may be necessary to resolve the higher order modes, which are outside the focus of this study but may be considered in a future study.

Free vibration with initial tip deflection experiments were also carried out for all of the cantilever beam samples with 0, 1, and 2 wt% loadings of the carbon nanotube types listed in Table 1 fabricated both with and without fiber reinforcement. Time series data of accelerometer output voltage collected from these tests are analyzed to characterize the damping by investigating the vibration envelope. An example acceleration time series is shown in Fig. 3 for a fiberglass reinforced sample with carbon nanotube fillers, in which the rectified accelerometer output in volts is shown with the peak values highlighted by circles. The series was converted to acceleration using the accelerometer calibration of 0.499 mV/m/s^2. Assuming a sinusoidal vibration and ignoring phase changes, the displacement can be computed as the ratio of the acceleration to the square of the frequency of vibration. The peak points of the displacement amplitude were empirically fit using the method of least-squared-error, to define the envelope of the form:

$$X(t) = X_o e^{-Bt^C t} = X_o e^{-Bt^{C+1}} \quad (1)$$

where X_o, B, and C are the fitting parameters, t is time, and $X(t)$ represents the amplitude of the beam tip displacement. Equation 1 represents an exponential decay of the amplitude consistent with viscous damping; however, the power law form of the exponential term Bt^C allows for representing the strain dependence of the damping such that for a purely viscous damping the parameter C is zero. Figure 3 shows only a single time series for clarity of the example; however, Eq. 1 was fit in a least-squared-sense to the peak points of five repeated experiments simultaneously. The epoxy matrix of the composite beams is a viscoelastic material giving rise to the primarily exponential decay seen in Fig. 3, and the damping of the epoxy is enhanced with the addition of carbon nanotubes.

Two representations of the system are considered here for the analysis of the experimental data: The first is a *linear spring-mass-damper* model, which is used to curve fit the experimental amplitude decay curves to find an effective damping ratio ζ_{eff}. It is often hypothesized in the literature [6, 10, 14–18] that the damping mechanism introduced by carbon nanotube fillers is because of stick slip friction between the carbon nanotubes and the surrounding matrix, which is in addition to the viscous damping inherent to the fiber reinforced composites. While the effective damping ratio reflects the combined effects of both these damping mechanisms, it is further instructive to isolate the contributions due to the two damping effects and study their respective trends with the carbon nanotube loading. To this end, the second representation considered is a *linear spring-mass-damper* system with dry friction, which is derived such that free vibration decrements of the

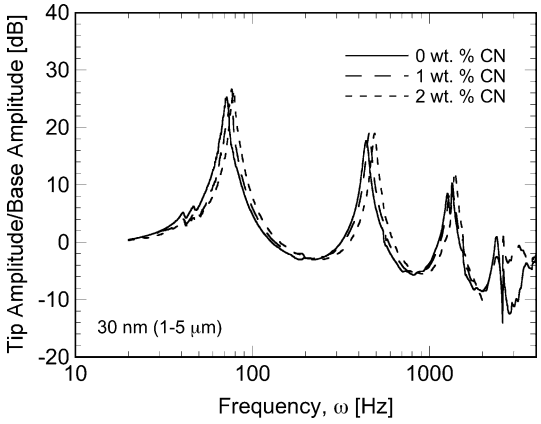

Fig. 2 Frequency response for 30 nm diameter 1–5 μm length carbon nanotube samples with 0, 1, and 2 wt% loadings in a fiber-reinforced epoxy beam

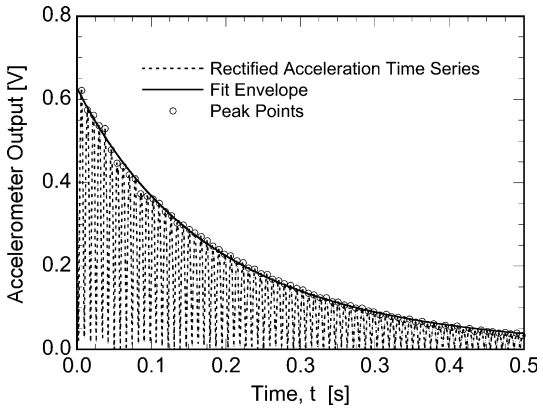

Fig. 3 Rectified time series of accelerometer voltage obtained from a free vibration with initial tip deflection experiment. The envelope represents a least squares fit through the peak point of the rectified series

system can be used to isolate viscous and dry friction. The analysis using each of the two representations is discussed in the following.

Analysis based on a linear spring-mass-damper model:

A *linear spring-mass-damper* model is used to characterize an effective damping ratio that combines the effects of viscous and Coulomb friction. For a *linear spring-mass-damper* system the amplitude decay envelope is of the form:

$$X(t) = X_o e^{-\zeta \omega_n t} \tag{2}$$

where X_0 is the initial amplitude of vibration, ζ is the damping ratio, and ω_n is the natural frequency of vibration. Comparison of Eqs. 1 and 2 reveals the following relation for the effective damping of the beam specimen:

$$\zeta_{\text{eff}} = \frac{Bt^C}{\omega_n} \tag{3}$$

in which, ζ_{eff} represents the damping ratio of the composite beam determined from comparisons of a lumped spring-mass-damper model with curve fits of the amplitude decay envelope through the experimental data. Physically, the time dependence shown in Eq. 3 can represent the strain dependence because the vibration amplitude monotonically decreases over time. The average surface strain of the cantilever beam was computed based on the tip displacement amplitude assuming the static deflected shape of the cantilever beam and considering the average strain at the surface of the beam on the tensile side [24].

The effective damping ratio, ζ_{eff}, is shown in Fig. 4 as a function of the average surface strain for a cantilever beam specimen with (a) no fiber reinforcement or carbon nanotubes (CN), (b) 2 wt% single-walled carbon nanotubes (SWCN), and (c) a dual scale reinforcement of both fiber and 2 wt% single-walled carbon nanotubes. All beams measured 4 inch in length and were tested with a 10 mm initial tip deflection. The pure resin sample shown as the solid line has an effective damping ratio (combined effect of viscous and Coulomb friction) that is nonlinearly strain dependent. The addition of carbon nanotubes (long dashed line) shows an increased ζ_{eff}; however, with the introduction of reinforcing fibers the damping ratio is reduced relative to the neat resin (short dashed line). The trend may be explained by the fact that in the fiberglass reinforced beam, strains local to the randomly oriented, relatively stiff fibers will be lower than the surrounding matrix and the carbon nanotubes in this region of local low strain are thus less likely to reach the critical strain at which stick slip friction will initiate. Overall this will lead to reduced Coulomb friction damping in fiber reinforced carbon nanotube filled composites. The reasoning is corroborated by the shift to higher natural frequencies with increased carbon nanotube content in the sine sweep experiments, Fig. 2, suggesting a good bonding between the high modulus carbon nanotubes and the surrounding matrix, and a corresponding reduction in the local strain field.

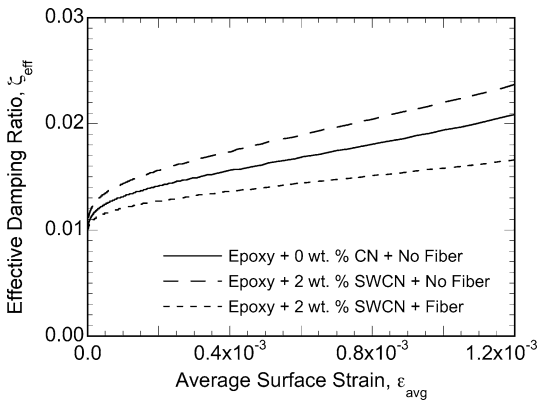

Fig. 4 Effective damping ratio, ζ_{eff} as a function of average surface strain, ε_{avg}, for samples comprised of epoxy (*solid line*), epoxy and 2 wt% SWCN (*large dashed line*), and epoxy, fiberglass reinforcement, and 2 wt% SWCN (*small dashed line*)

It may be argued that a decrease in the resin content due to the presence of approximately 18% fiber in the dual-scale reinforced sample compared to the sample with only SWCN could be a reason for the reduced damping. However, as seen for the larger strain in Fig. 4, the sample with only SWCN and no fiber shows a 45% augmentation in damping than the dual-scale reinforced sample, which is more than what could be accounted for by a volumetric resin deficit, suggesting that the damping reduction because of the extra stiffness arising from glass fibers is the dominant mechanism in comparison to any effect of the reduction in the resin content. Alternatively, the increased stiffness could be because of changes in the polymer properties near the nanotubes, as suggested in refs. [11–13]. Further investigations on delineating the physics underlying the observed phenomena are warranted in a future study.

The free vibration with initial tip deflection test used to obtain the results presented above mainly excites the primary mode of vibration and thus the results do not consider damping contributions from higher frequencies. Figure 5 shows the effective damping ratio results of free vibration tests with initial tip deflection of 20 mm, for a range of vibrational frequencies obtained by changing the cantilevered length of the 2 wt% single-wall carbon nanotube sample with fiber reinforcement. Tests were performed with beam lengths from 3.5–5 inches at every 0.5 inch increment and in each case the strain corresponding to a deflected configuration was calculated as explained previously. The results indicate a nonlinear strain dependence

for all beam lengths tested where the effective damping ratio increases with increasing strain; ζ_{eff} also shows a frequency dependence where the effective damping is greater at higher frequencies.

Analysis based on a linear spring-mass-damper model with dry friction:

Since the inclusion of carbon nanotubes is postulated in the literature [6, 10, 14–18] to introduce damping by Coulomb friction in addition to the viscous damping, it is instructive to isolate the contributions due to the two damping effects and study their respective trends with the carbon nanotube loading. To this end, an approach based on the decrement method as originally proposed in [25, 26] was used to isolate the effects of Coulomb and viscous friction. The method will be briefly summarized here; however, the interested reader is referred to [25, 26] for a more complete description. The equation of motion of a spring-mass-damper with dry contact has the form:

$$m\ddot{x} + c\dot{x} + kx + f(\dot{x}) = 0, \tag{4}$$

where m, c, and k are the mass, viscous damping coefficient, and spring stiffness respectively, x is the displacement of the mass relative to the unstretched spring position, and $f(\dot{x})$ represents the dry friction: $f(\dot{x}) = f_k \cdot sign(\dot{x})$, $\dot{x} \neq 0$, and $-f_s \leq f(0) \leq f_s$. Equation 4 is individually solvable for regions of $\dot{x} > 0$ and $\dot{x} < 0$. In addition, the equilibrium position changes, which necessitates an iterative solution as follows.

From initial conditions of $x(t_o) = X_o > x_s = f_s/k$, where x_s and f_s represent the maximum equilibrium displacement and maximum static friction force respectively, and $\dot{x}(t_o) = 0$, the motion will start in the negative direction and takes on the form:

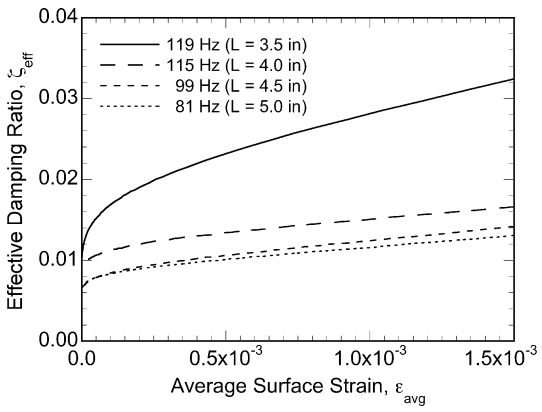

Fig. 5 Effective damping ratio, ζ_{eff}, as a function of average surface strain, ε_{avg}, for fiber reinforced composite samples with 2 wt% SWCN at varying beam lengths

$$x(t) = (X_0 + x_k)e^{-\zeta\omega_n(t-t_0)}. \\ (\cos\omega_d(t-t_0) + \beta\sin\omega_d(t-t_0)) + x_k, \tag{5}$$

where $\omega_d = \omega_n\sqrt{1-\zeta^2}$, $\beta = \zeta/\sqrt{1-\zeta^2}$, x_k is the dry friction parameter, and $\omega_n = \sqrt{k/m}$ is the natural frequency of vibration. Motion will continue until $\dot{x} = 0$ at which time $X_1 = x(t_1) = -e^{-\beta\pi}X_o + \left(e^{-\beta\pi} + 1\right)x_k$. If $X_1 < -x_s$, the mass will continue sliding on the opposite direction according to the solution:

$$x(t) = (X_1 + x_k)e^{-\zeta\omega_n(t-t_1)}. \\ (\cos\omega_d(t-t_1) + \beta\sin\omega_d(t-t_1)) - x_k, \tag{6}$$

until $\dot{x} = 0$ and so on until the stopping position, X_n is smaller than x_s. This iterative process yields a relation for the peaks and valleys of oscillation defined as:

$$X_i = -e^{-\beta\pi}X_{i-1} + (-1)^{i-1}\left(e^{\beta\pi} + 1\right)x_k, i = 1, 2, \ldots, n. \tag{7}$$

From Eq. 7, a ratio of the difference of successive peaks and valleys can be written in the following decrement form [25, 26]:

$$\frac{X_{i+1} - X_{i-1}}{X_i - X_{i-2}} = -e^{-\beta\pi} \tag{8}$$

that is used to define β which is directly related to the viscous damping ratio, ζ. Following the identification of β, the dry friction parameter, x_k, can be evaluated from Eq. 7, where X_i is determined by evaluating Eq. 1 at successive half periods based on an averaging of the five repeated experiments through the curve fitting method described above.

The meaning of the dry friction parameter, x_k, can be inferred from the decrement method by examining a system in the absence of viscous damping. For the viscous damping factor $\beta = 0$, Eq. 7 reduces to: $X_i = -X_{i-1} + (-1)^{i-1}2x_f$, which states that the absolute value of the dissipation over a half period (i to $i-1$) is $2x_f$ (this equation defines the slope of the decay envelope in the absence of viscous damping). Using this relation, the specific damping capacity, defined as the kinetic energy dissipated in a cycle divided by the maximum kinetic energy for that cycle [27], can be computed as a measure of the damping. The kinetic energy (KE) takes on the form $KE = 0.5m\dot{X}^2$ where m is the lumped mass and $\dot{X}$ is the amplitude of the velocity. The maximum kinetic energy for a period occurs when there is no dissipation over the period such that $KE_{max} = .5m(X_i\omega)^2$, and the dissipated kinetic energy over a period can be written as: $KE_{dis} = .5m((X_i\omega)^2 - (X_i\omega - 4x_f\omega)^2)$ where the change in velocity is computed from the slope of the Coulomb friction decay envelope.

Taking the ratio of KE_{dis} and KE_{max} the specific damping capacity, ψ, is written as:

$$\psi = 1 - \left(1 - 4x_f/X_i\right)^2 \tag{9}$$

Initial tip deflection tests performed on the cantilever beam samples with fiber reinforcements were analyzed with the decrement method [25, 26] outlined above to determine the viscous damping ratio, ζ, plotted in Fig. 6a–d and the dry friction parameter, x_k, used to compute the specific damping capacity, ψ, plotted in Fig. 7a–d. The four frames in each of these figures represent results from 5 inch long fiber reinforced beams produced with (a) single-walled carbon nanotubes, (b) 15 nm diameter, 5–20 μm length multi-walled carbon nanotubes, (c) 30 nm diameter, 5–20 μm length multi-walled carbon nanotubes, and (d) 30 nm diameter, 1–5 μm length multi-walled carbon nanotubes. The damping ratio, ζ is plotted as a function of average surface strain for 0, 1, and 2 wt% carbon-nanotube filler content. The tests were conducted for initial tip displacements of 5, 10, and 20 mm, which progressively increased the range of the average surface strain on the samples. All of these tests revealed a generally similar trend except for the range of the strain values. For brevity, only the results for the largest tip deflection of 20 mm are shown in Fig. 6. Since this analysis separates the viscous damping introduced by the viscoelastic epoxy and the Coulomb damping introduced by the stick-slip friction at the carbon nanotube-epoxy interface, it is expected that the viscous damping ratio would be unchanged with the addition of carbon nanotubes. This is generally evident in Fig. 6a–d where the maximum variation in the damping ratio with respect to carbon nanotube loading is within about 15% relative to a mean value, and is considered to be within the range of experimental uncertainty and accuracy of the empirical fitting of the parameters in the calculation of X_i's in Eq. 8. All of the specimens tested and reported in Fig. 6 show a nonlinear increase of the damping ratio with strain.

Figure 7 shows the specific damping capacity, ψ, as a function of average surface strain for fiber reinforced samples with the carbon-nanotube fillers listed in Table 1 at 0, 1, and 2 wt%. For the damping mechanism of stick-slip friction, the damping introduced by the addition of carbon nanotubes would be expected to increase with increasing effective surface area for interfacial slip. Table 1 indicates the surface area to weight ratio of the carbon nanotubes studied here; the effective surface area was calculated excluding the ends of the tube structure and the weight is calculated using the average length and cross sectional area of the carbon nanotube and a constant density for carbon. Figure 7a presents the results for samples produced with single-walled nanotube fillers, offering the largest surface area to weight ratio of 1709 m^2/g and correspondingly the largest specific damping capacity at each weight percent studied. With 2 wt% single-wall carbon nanotube content the damping capacity has increased almost 100% over the neat resin sample at the largest average surface strain studied, $\zeta_{avg} = 0.0012$. Samples produced with multi-walled nanotubes with a 15 nm diameter and 1–5 μm length offer the next largest surface area to weight ratio of 148 m^2/g and correspondingly the next largest specific damping capacity at each wt%, as shown in Fig. 7b. At the maximum studied average surface strain the increase in specific damping capacity is seen to be 67%. The two multi-walled carbon nanotube lengths with a diameter of 30 nm share a surface area to weight ratio of 74 m^2/g and as such samples produced with these carbon nanotubes would be expected to have similar specific damping capacities as is seen in Fig. 7c, d; the minimal variation of specific damping capacity with nanotube content is on the order of 15% which is within the range of the experimental uncertainty.

In general the damping seen in the results presented above is low compared to results presented by others [6]. This may be attributed to the resin-carbon-nanotube bond being relatively strong in this study partly because of the different resin and curing agent used as well as owing to the molding technique. The increased bond strength is validated by the rise in stiffness with carbon nanotube content shown by the higher natural frequencies in the sine sweep experiments (Fig. 2). To further explore the strength of the bond between the carbon-nanotube fillers and the epoxy matrix, the produced ASTM 683 type V specimens were tested for stiffness in an INSTRON tension testing machine as outlined in Tensile testing. Figure 8 shows the modulus of the composite samples with fiberglass reinforcement as a function of the weight percent of carbon nanotube filler. The variation in modulus for the five experiments per sample and two samples per carbon nanotube type and loading are represented by the two standard deviation error bars. Variation of carbon nanotube type did not reveal any trends so the 1 and 2 wt% error bars represent all four types of carbon nanotubes at that loading. The stiffness increases with the addition of carbon nanotubes indicating the existence of bonding between the carbon nanotubes and epoxy matrix further validating the hypothesis that limited damping is seen for the produced samples because of the superior bonding and thus lack of sites for the existence of Coulomb friction.

In order for stick slip fiction to occur, the carbon nanotubes must partially release from the surrounding matrix. It has been reported in the literature that a minimum stress exists below which debonding will not occur and thus the frictional damping mechanism is lost. In this study, the minimum stress for debonding may be elevated

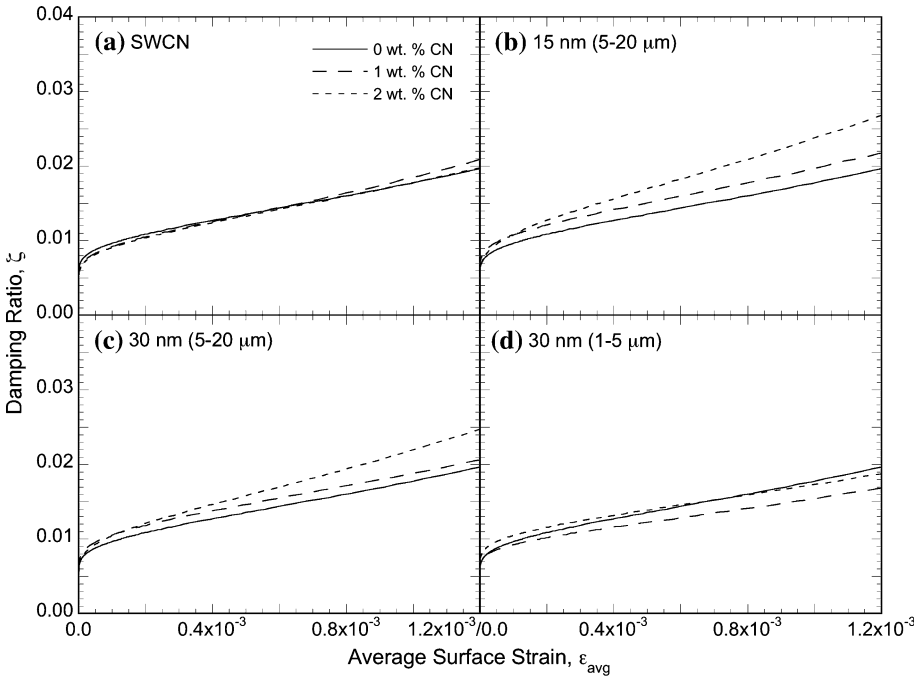

Fig. 6 Viscous damping ratio, ζ, plotted as a function of the average surface strain, ε_{avg}, for glass fiber reinforced composite cantilever beams filled with **a** single-wall carbon nanotubes, **b** 15 nm diameter 5–20 μm length carbon nanotubes, **c** 30 nm diameter 5–20 μm length carbon nanotubes, and **d** 30 nm diameter 1–5 μm length carbon nanotubes

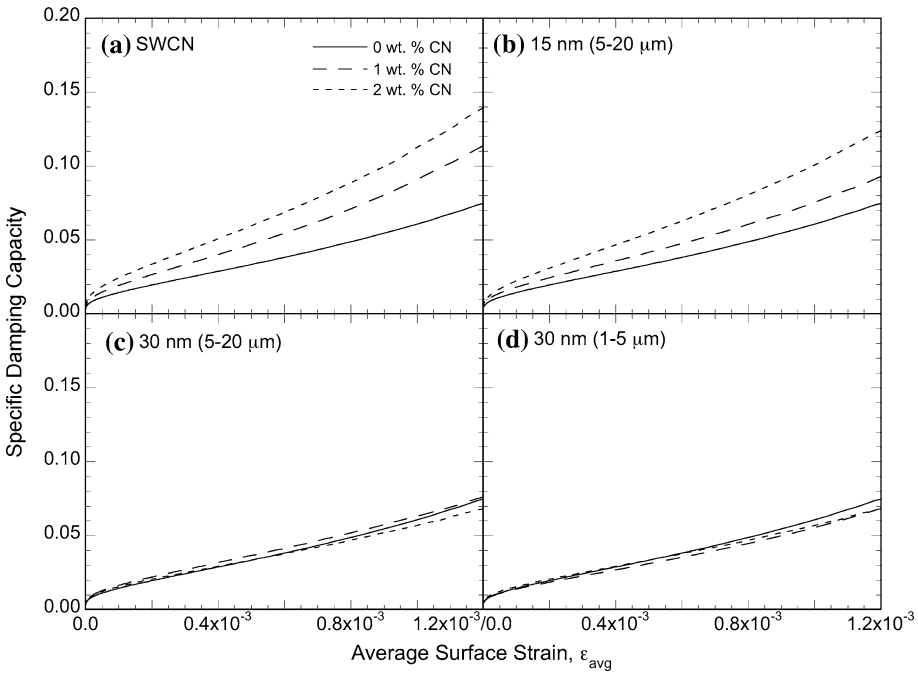

Fig. 7 Specific damping capacity, ψ, plotted as a function of the average surface strain, ε_{avg}, for glass fiber reinforced composite, cantilever beams filled with **a** single-wall carbon nanotubes, **b** 15 nm diameter 5–20 μm length carbon nanotubes, **c** 30 nm diameter 5–20 μm length carbon nanotubes, and **d** 30 nm diameter 1–5 μm length carbon nanotubes

by the molding technique or the local stress seen by a nanotube could be below the critical value for debonding because of the nanotubes orientation, location inside the beam or proximity to a reinforcing fiber. Future modeling work and experimental investigation of dispersion is needed to determine the true cause. The testing method of initial tip release may also contribute to the relatively low strain when compared to uniaxial tension testing methods as the maximum strain will only be seen at the extremities of the beam thickness and not uniformly throughout as in uniaxial testing methods. Also the transient nature of a free vibration with initial tip deflection test has very limited data at higher strains even at large initial tip deflections. Forced uniaxial testing methods may be used in future work to study the ASTM 683 type V specimens; however, the larger strains characteristic of this method may not be practical for the majority of applications of the studied samples. At low strain, increased temperature may reduce

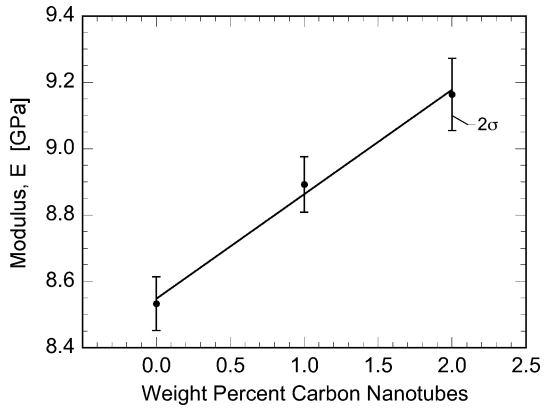

Fig. 8 Young's modulus for samples with varying weight percent of carbon nanotube filler in fiber reinforced composites

the critical stress at which debonding occurs [15] and provide a source of useful applications for these materials.

The carbon nanotube aspect ratio reported in the study was based on the length and diameter information of the as-purchased samples provided by the manufacturer. It is expected that the nanotubes will undergo some breakage during ultrasonic dispersion, and further during composites processing. The aspect ratios measured post sonication and post processing will shed additional light on correlating the damping behavior to the true aspect ratio in the final specimens, and will be conducted in a future study. Furthermore, detailed microstructural characterization of dispersion after sonication and after processing are needed to identify such effects as any tendency of nanotubes to be attracted to (or repulsed) from the glass fiber surface, which could, in turn affect the damping behavior. These issues as well as damping in composites with higher fiber volume fraction will be addressed in a future work.

Conclusions

An experimental study of the damping introduced by carbon-nanotube fillers in a structural thermosetting epoxy matrix fiberglass reinforced composite was presented. The components of damping because of viscous and Coulomb friction were separately quantified in terms of the viscous damping ratio and the specific damping capacity respectively. Results of free vibration with initial tip deflection tests show increased Coulomb friction damping with increasing nanotube content as well as with increasing surface area to weight ratio as demonstrated by studying a range of carbon nanotube weight percentages and geometries. It was also seen that the introduction of fibers reduces the effective damping ratio that is otherwise enhanced by the addition of carbon-nanotube fillers. Overall the study presented for the first time the effects of carbon nanotubes on damping in fiber-reinforced composites and a comparative analysis relative to damping in carbon-nanotube filled resins without fiber reinforcements.

Acknowledgements The authors acknowledge Owens Corning for providing gratis the fiberglass preform material used in this study.

References

1. Liao W, Wang KW (1997) J Sound Vib 207(3):319
2. Nayfeh S (2004) J Sound Vib 276:689
3. Ajayan PM, Schadler LS, Giannaris C, Rubio A (2000) Adv Mater 12(10):750
4. Breuer O, Sundararaj U (2004) Polym Compos 25(6):630
5. Xu Y, Ray G, Abdel-Magid B (2006) Comp Appl Sci Manufac 37:114
6. Zhou X, Shin E, Wang KW, Bakis CE (2004) Compos Sci Technol 64:2425
7. Koratkar N, Wei B, Ajayan PM (2002) Adv Mater 14(13,14):997
8. Wei C (2006) Appl Phys Lett 88:042905
9. Schadler LS, Giannaris SC, Ajayan PM (1998) Appl Phys Lett 73(26):3842
10. Zhou X, Wang KW (2004) Proc SPIE 5386:162
11. Ding W, Eitan A, Fisher F, Chen X, Dikin D, Andrews R, Brinson L, Schadler L, Ruoff R (2003) Nano Lett 3(11):1593
12. Fisher F, Eitan A, Andrews R, Schadler L, Brinson L (2004) Adv Comp Lett 13(2):105
13. Eitan A, Fisher F, Andrews R, Brinson L, Schadler L (2006) Compos Sci Technol 66:1159
14. Koratkar NA et al. (2005) Appl Phys Lett 87
15. Suhr J, Zhang W, Ajayan PM, Koratkar NA (2006) Nano Lett 6(2):219
16. Koratkar NA, Wei B, Ajayan PM (2003) Compos Sci Technol 63:1525
17. Rajoria H, Jalili N (2005) Compos Sci Technol 65:2079
18. Mahmoodi SN, Khadem SE, Jalili N (2006) Arch Appl Mech 75:153
19. Suhr J, Koratkar N, Keblinski P, Ajayan P (2005) Nat Mater 4:134
20. Suhr J, Schadler L, Koratkar N (2005) Proc SPIE 5760:164
21. Standard test method for tensile properties of plastics, ASTM D638–02a, Annual Book of ASTM Standards, vol. 8.01 (2005)
22. Rao SS (1995) Mechanical Vibrations, 3rd edn. Addison-Wesley, New York
23. Adhikari S (2000) Damping models of structural vibration. Ph.D. Dissertation, Cambridge University, Cambridge
24. Beer FP, Johnston ER (1992) Mechanics of materials, 2nd en. McGraw-Hill, New York
25. Feeny BF, Liang JW (1996) J Sound Vib 195(1):149
26. Liang JW, Feeny BF (1998) Nonlin Dynam 16:337
27. Nashif AD (1985) Vibration Damping. Wiley, New York